UNDERSAMPLED DYNAMIC FOURIER PTYCHOGRAPHY VIA PHASELESS PCA

Zhengyu Chen, Seyedehsara (Sara) Nayer, Namrata Vaswani

Iowa State University, Ames, IA, USA.

2022 IEEE International Conference on Image Processing (ICIP) | 978-1-6654-9620-9/22/$31.00 ©2022 IEEE | DOI: 10.1109/ICIP46576.2022.9897747

ABSTRACT

In recent work, we studied the phaseless PCA (low rank phase retrieval) problem and developed a provably correct and fast alternating minimization (AltMin) solution for it called AltMinLowRaP. In this work, we develop a modification of AltMinLowRaP, called AltMinLowRaP-Ptych, that is designed for reducing the sample complexity (number of measurements required for accurate recovery) for dynamic Fourier ptychographic imaging. Fourier ptychography is a computational imaging technique that enables high-resolution microscopy using multiple low-resolution cameras. Via exhaustive experiments on real image sequences with simulated ptychographic measurements, we show the power of our algorithm for reducing the number of samples required for accurate recovery.

***Index Terms*—** Phase retrieval, Fourier ptychography, low rank

1. INTRODUCTION

A common problem in microscopy and long-distance imaging is diffraction blurring. Fourier ptychography [1] is a technique which mitigates its effects by constructing a large synthetic aperture. Practically, this setup can be implemented by either spatially moving a single camera [2], or by an array of fixed cameras [1], similar to those used in light-field cameras; each of the cameras measures different parts of the Fourier spectrum of the desired images. The image formed at the sensing plane is complex-valued due to phase shifts induced by the optical lens setup. The sensing apparatus is incapable of estimating the phase of the complex values, and only the magnitudes can be measured. From a signal processing perspective [3, 4], after some standard pre-processing, each camera's measurement can be modeled as the magnitude of a different bandpass filtered version of the unknown high-resolution image. The image reconstruction problem can thus be posed as one of phase retrieval (PR): recover the unknown vectorized image $\mathbf{x}$ from $\mathbf{y} := |\mathbf{A}\mathbf{x}|$ where $|.|$ denotes element-wise magnitude and $\mathbf{A}$ is the (known) matrix corresponding to the measurement process.

To get enough measurements per image, one either needs many cameras, or one needs to move a single camera to different locations to acquire the different bands. This can make the acquisition process expensive or very slow. There has thus been significant interest in exploiting structural assumptions such as sparsity or low-rank (LR) to reduce the number of cameras (or camera movements) required [4]. When considering dynamic imaging, e.g., imaging of live biological specimens, joint reconstruction of a set of similar images is needed. In this case, a low rank (LR) assumption on the matrix formed by arranging the images as its columns is a more flexible model than sparsity or joint sparsity, since it does not require knowledge of the sparsifying basis or dictionary. Natural image sequences typically change slowly over time; hence the matrix formed by the vectorized images as its columns is well-modeled as being approximately LR. With imposing an LR assumption, the dynamic Fourier ptychographic imaging problem becomes one of "Phaseless PCA" or "low rank PR (LRPR)"; this was explored extensively in our recent work [5, 6, 7]. We developed a fast AltMin approach called AltMinLowRaP that, in simulation experiments, significantly improved upon our older approach from [5, 4], and that also comes with stronger theoretical guarantees (all guarantees are for i.i.d. random Gaussian $\mathbf{A}_k$s).

Contribution: In this work, we develop a modification of the basic AltMinLowRaP approach, called AltMinLowRaP-Ptych, and show its advantage our existing approaches for undersampled dynamic Fourier ptychographic imaging. AltMinLowRaP-Ptych needs a different initialization approach since the original one was developed for random Gaussian measurements. It also includes an extra LR model correction step to deal with the fact that real image sequences are not exactly LR. We show the significant advantage of our approach over both our older algorithm from [5, 4] (LR-Ptych), as well as over other standard PR [3], sparse PR [4] and block sparse PR based solutions, for recovering multiple real image sequences from simulated Fourier ptychographic measurements at different undersampling ratios.

Other Related Work. Other somewhat related work on use of PR in imaging applications includes [8, 9, 10, 11, 12].

2. PROBLEM FORMULATION

We first give the general problem definition next and then explain the Fourier ptychographic setting.

2.1. Low Rank PR (Phaseless PCA)

Low Rank PR (LRPR) involves recovering an $n \times q$ rank-r matrix $\mathbf{X}^* = [\mathbf{x}_1^*, \mathbf{x}_2^*, \dots, \mathbf{x}_k^*, \dots, \mathbf{x}_q^*]$ with $r \ll n, q$ (LR), from different phaseless linear projections of each of its columns, i.e., from

$$\mathbf{y}_k := |\mathbf{A}_k \mathbf{x}_k^*|$$

where the $\mathbf{A}_k$s are *known* $m \times n$ measurement matrices, and $|\mathbf{v}|$ takes element-wise magnitude of each entry of $\mathbf{v}$.

Observe that our measurements are not global, i.e., no scalar measurement (one entry of $\mathbf{y}_k$) is a function of the entire matrix $\mathbf{X}^*$. The measurements are global for each column, but not across the different columns. We thus need the following incoherence assumption to enable correct interpolation across the different columns [6]. This was introduced in [13] for LR matrix completion (LRMC) which is another LR problem with non-global measurements.

Right singular vectors' incoherence: We assume that $\max_k \|\mathbf{x}_k^*\|^2 \leq \tilde{\mu} \sum_{k=1}^q \|\mathbf{x}_k^*\|^2/q$ for a constant $\tilde{\mu} \geq 1$ but not too large[1]. This is requiring that the "energy" (squared 2-norm) of the various images, $\mathbf{x}_k^*$, is similar so that the maximum energy is within a constant factor of its average value. This is valid for most natural image sequences that changes slowly over time.

2.2. Approx-LRPR for real image sequences

Real image sequences are only approximately LR. Thus, the model

$$\mathbf{y}_k = |\mathbf{A}_k \mathbf{z}_k^*|, \text{ with } \mathbf{z}_k^* = \mathbf{x}_k^* + \mathbf{e}_k^*,$$

$\mathbf{x}_k^*$s forming an LR matrix $\mathbf{X}^*$, and $\mathbf{e}_k^*$ being the small residual in this model, is more practically valid one than exact LRPR described above. In particular we assume that $\|\mathbf{e}_k^*\| \ll \|\mathbf{x}_k^*\|$. Here $\mathbf{z}_k^*$ now is the vectorized unknown image that needs to be recovered. We use this model in the current work.

2.3. Fourier Ptychography as an approx-LRPR problem

In the description below we use $(\mathbf{z})_{img}$ to refer to the 2D image version of an n-length vector $\mathbf{z}$. As explained in detail in [15, 3], for an image, $(\mathbf{z})_{img}$, the imaging model is

$$\mathbf{y}_i = |\mathcal{F}^{-1}(\mathcal{P}_i(\mathcal{F}((\mathbf{z})_{img}))|, \ i = 1, \dots, N$$

where $\mathcal{F}$ and $\mathcal{F}^{-1}$ represent the 2D discrete Fourier transform and inverse-DFT operators, $\mathcal{P}_i$ is the pupil mask corresponding to the i-th camera (or LED): it models the bandpass filtering operation: selects a region of the Fourier spectrum while zeroing out the rest of it (different regions are selected for different i). The image obtained by the i-th camera, $\mathbf{y}_i \in \mathbb{C}^n$ for simplicity of notation (although the information content in it is less than n). The stack of measurements corresponding to all N cameras $\mathbf{y} \in \mathbb{C}^{nN}$.

Our undersampling approach consists of using images from a subset of the cameras. A different subset is used for different images k in the sequence. We model this by using a mask $\mathcal{M}_{i,k}(.)$ which either returns its argument or zeros depending on if the camera is selected or not. Thus, for an image sequence matrix $\mathbf{Z}^*$, for each column k, we measure

$$\mathbf{y}_{i,k} = \mathcal{M}_{i,k}(\mathcal{F}^{-1}(\mathcal{P}_{i,k}(\mathcal{F}((\mathbf{z}_k^*)_{img})))) := \mathcal{A}_{i,k}((\mathbf{z}_k^*)_{img})), \ i \in [N]$$

As above, $\mathcal{P}_{i,k}(.)$ is the pupil mask that models the bandpass filtering operation. The cameras' mask $\mathcal{M}_{i,k}$ can either select a subset of cameras or pixels from each camera. The former is a more practically useful setting and hence we use that in our current experiments. In either case, the sampling scheme is such that the central camera (camera corresponding to the low-pass filtering operation) is always selected. Fig. 1 shows $\mathcal{A}_{i,k}((\mathbf{z})_{img})$ and $\mathcal{A}_{i,k}^\top(\mathbf{y})$.

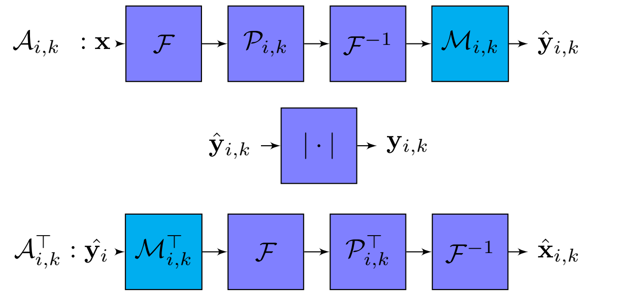

Fig. 1: *Operator $\mathcal{A}_{i,k}$ and $\mathcal{A}_{i,k}^\top$. $\mathcal{M}_{i,k}^\top(.)$ returns a zero vector if camera i was not selected, and returns its argument otherwise. $\mathcal{P}_{i,k}^\top(.)$ zeros out the entries of its input corresponding to parts of the Fourier spectrum that were turned off.*

With the above model, $\mathbf{y}_k = [\mathbf{y}_{1,k}^\top, \mathbf{y}_{2,k}^\top, \dots, \mathbf{y}_{N,k}^\top]^\top$, $\mathcal{A}_k$ is a similar concatenation of $\mathcal{A}_{i,k}$ for $i \in [N]$, and $m = nN$.

We should clarify here that, when linear operators or transforms are applied on an image, the entire operation can always be expressed as a matrix-vector multiplication for the vectorized image. However, computationally, directly applying the operators/transforms is much faster. Also it is easier to understand from a practitioner's perspective. Thus, in the writing above, $\mathbf{y}_k := |\mathbf{A}_k \mathbf{z}_k^*|$ is replaced by $\mathbf{y}_{i,k} = |\mathcal{A}_{i,k}((\mathbf{z}_k^*)_{img})|, \ i \in [N]$.

Notice that the above problem setting is different from the random Gaussian setting where $m \ll n$ suffices. The reason is the different entries/pixels of each captured image $\mathbf{y}_{i,k}$ are highly correlated ($\mathbf{y}_{i,k}$s are low-resolution images), whereas in the random Gaussian case, the different scalar entries of $\mathbf{y}_k$ are mutually independent.

3. THE PROPOSED ALGORITHM: ALTMINLOWRAP-PTYCH

Our proposed approach (Algorithm 1) is inspired by the AltMinLowRaP algorithm from our older work [7]. It expresses the estimate of the unknown matrix as $\mathbf{X} = \mathbf{U}\mathbf{B}$ where $\mathbf{U}$ is $n \times r$, $\mathbf{B}$ is $r \times q$, and considers the squared loss cost function

$$f(\mathbf{U}, \mathbf{B}) := \sum_k \|\mathbf{y}_k - |\mathcal{A}_k((\mathbf{U}\mathbf{b}_k)_{img})|\|_2^2$$

[1]Treating the condition number of $\mathbf{X}^*$ as a constant, this assumption implies incoherence [13, 14] of the right singular vectors of $\mathbf{X}^*$ with incoherence parameter $\tilde{\mu}\kappa$, in the traditional sense. We state it this way, to make its interpretation easier for the current work.

AltMinLowRaP uses a spectral initialization approach to obtain the first estimate of $\mathbf{U}$. It then uses AltMin to update $\mathbf{B}$ and $\mathbf{U}$ alternatively by minimizing $f(\mathbf{U}, \mathbf{B})$ over one keeping the other constant. The update of $\mathbf{U}$ is followed by an orthonormalization step to prevent the norm of one of them from growing (or decreasing) in an unbounded fashion. The update of $\mathbf{B}$ is clearly decoupled across columns, each is updated by solving a standard r-dimensional noisy PR problem with measurement vector $\mathbf{y}_k$ and measurement operator $\mathcal{A}_k((\mathbf{U}\cdot)_{img})$. We use the AltMinPhase algorithm of [16] for this standard PR step. This is specified in Algorithm 2. Other methods such Truncated or Reshaped Wirtinger Flow can also be used instead. The update for $\mathbf{U}$ is a non-standard PR problem but it can be simplified using the following insight: when estimating $\mathbf{b}_k$'s by standard PR, we also obtain an estimate of the measurement phases: if we use a diagonal matrix $\mathbf{C}_k$ to denote these estimates, then $\mathbf{C}_k := diag(\mathcal{A}_k((\mathbf{U}\mathbf{b}_k)_{img}))$; here $diag(v)$ makes a diagonal matrix using the entries of the vector v. Given $\mathbf{C}_k$ and $\mathbf{b}_k$, we can minimize $\sum_k \|\mathbf{C}_k \mathbf{y}_k - \mathcal{A}_k((\mathbf{U}\mathbf{b}_k)_{img})\|_2^2$ over $\mathbf{U}$: this is a standard least squares (LS) problem. For our current application, we need two changes to the above approach.

Initialization. The spectral initialization step was designed for i.i.d. Gaussian matrices and does not work in the current setting. To address this, we use a simple modification of the approach we developed in [4]. We compute $\hat{\mathbf{x}}_k^0 = \sqrt{\frac{1}{N}\sum_{i=1}^N \mathbf{y}_{i,k}.^2}$, where $\mathbf{y}_{i,k}.^2$ means element-wise square, use this to define that matrix $\mathbf{X}^0$, compute its r-SVD (top r left singular vectors), and use this as an estimate of $\mathbf{U}^0$.

Model Error Correction (MEC) step. Second, since the matrices formed by real image sequences are only approximately LR, we need a model error correction (MEC) step. First, we estimate the LR matrix $\mathbf{X}^*$ using the measurements $\mathbf{y}_k$ as input to the basic AltMinLowRaP algorithm. Next, we estimate the unstructured small residual $\mathbf{e}_k^*$ by minimizing

$$\|\mathbf{y}_k - |\mathcal{A}_k((\mathbf{x}_k^{final} + \mathbf{e})_{img})|\|_2^2 + \tau\|\mathbf{e}\|_2^2$$

using an AltMin approach that minimizes over $\mathbf{e}$ and the phases' matrix $\mathbf{C}_k$ alternatively: it solves $\min_{\mathbf{e},\mathbf{C}} \|\mathbf{C}\mathbf{y}_k - \mathcal{A}_k((\mathbf{x}_k^{final} + \mathbf{e})_{img})|\|_2^2 + \tau\|\mathbf{e}\|_2^2$ by AltMin with a zero initialization of $\mathbf{e}$ as the starting point. This is specified in Algorithm 3.

The complete algorithm is summarized in Algorithm 1.

Algorithm 1 AltMinLowRaP-Ptych

(Initialization)

Input: $\mathbf{y}_k, \mathcal{A}_{i,k}, r$

$\hat{x}_k^0 \leftarrow \sqrt{\frac{1}{N}\sum_{i=1}^N y_{i,k}^2}$, k indexes frames, $k = 1, \ldots, q$.

$[\hat{\mathbf{U}}^0, \mathbf{S}^0, \mathbf{V}^0] \leftarrow ReducedSVD((X^0), r)$

(Low-rank matrix recovery)

for $t = 1, 2, \ldots, T$ **do**

  $\hat{\mathbf{B}}^t \leftarrow$ output of Algorithm 2

  $\hat{\mathbf{X}}^t = \hat{\mathbf{U}}^{t-1}\mathbf{B}^t$

  $\hat{\mathbf{C}}_k^t \leftarrow \mathrm{diag}(phase(\mathcal{A}_k(\hat{\mathbf{U}}^{t-1}\hat{\mathbf{b}}_k^{t-1})))$, $k = 1, \ldots, q$

  $\hat{\mathbf{U}}^{tmp} \leftarrow \arg\min_{\tilde{\mathbf{U}}} \sum_k \|\hat{\mathbf{C}}_k^t \mathbf{y}_k - \mathcal{A}_k(\tilde{\mathbf{U}}\hat{\mathbf{b}}_k^{t-1})\|^2$

  $\hat{\mathbf{U}}^t \leftarrow QR(\hat{\mathbf{U}}^{tmp})$

end for

(Modeling-error correction)

$\hat{\mathbf{Z}}_{MEC}^{T'} \leftarrow$ output of Algorithm 3 using $\mathbf{X}^{final} = \hat{\mathbf{X}}^T$ as one of its inputs.

Algorithm 2 Update of $\mathbf{b}_k$ using AltMinPhase [16]

Input: $\mathbf{y}_k, \mathcal{A}_{i,k}, \hat{\mathbf{U}}^{t-1}, \hat{\mathbf{X}}^{t-1}, T_b$

$\hat{\mathbf{B}}_{init} = \hat{\mathbf{U}}^{t-1\top}\mathbf{X}^{t-1}$

for $t_b = 1, 2, \ldots, T_b$ **do**

  for $k = 1, \ldots, q$ **do**

    $\hat{\mathbf{C}}_k^{t_b} \leftarrow \mathrm{diag}(phase(\mathcal{A}_k(\hat{\mathbf{U}}\hat{\mathbf{b}}_k^{t_b-1})))$

    $\hat{\mathbf{b}}_k^{t_b} \leftarrow \arg\min_{\tilde{\mathbf{b}}_k} \|\hat{\mathbf{C}}_k^{t_b}\mathbf{y}_k - \mathcal{A}_k(\hat{\mathbf{U}}\tilde{\mathbf{b}}_k)\|^2$

  end for

end for

Algorithm 3 Model Error Correction (MEC) step

Input: $\mathbf{y}_k, \mathcal{A}_{i,k}, \mathbf{X}^{final}, T'$

for $k = 1, \ldots, q$ **do**

  $\mathbf{e}_k^0 \leftarrow \mathbf{0}$

  for $t = 1, 2, \ldots, T'$ **do**

    a) $\hat{\mathbf{C}}_k^t \leftarrow \mathrm{diag}(phase(\mathcal{A}_k(\hat{\mathbf{z}}_k^t)))$

    b) $\mathbf{e}_k^t \leftarrow \arg\min_{\mathbf{e}}(\|\hat{\mathbf{C}}_k^t\mathbf{y}_k - \mathcal{A}_k(\hat{\mathbf{x}}_k^{final} + \mathbf{e})\|_2^2 + \tau\|\mathbf{e}\|_2^2)$

    c) $\hat{\mathbf{z}}_k^{t+1} = \mathbf{x}_k^{final} + \mathbf{e}_k^t$

  end for

end for

4. EXPERIMENTAL RESULTS

We compare our algorithm with existing approaches on synthetically produced measurements of real videos. We used 4 videos: 'Bacteria" (B),"Fish"(F), and "Mouse"(M), and "Plane" (P). Videos are of size $180 \times 180 \times q$ with different number of frames q for each video. Number of frames are $q = 105, 112, 88, 90$ for videos of "P","B", "F", and "M" respectively. The camera array consists of $N_{full} = 81$ cameras (9×9 array) with aperture size of 40 pixels and overlap of 0.7 between consecutive cameras, similar with [3].

Our undersampling mask is generated as follows. The central camera (camera corresponding the low-pass filtering operation) is always selected for each frame. The rest are chosen as follows.

$$\mathcal{M}_{i,k}(\mathbf{v}) = u_{i,k}\mathbf{v}$$

where $Pr(u_{i,k} = 1) = f$ and $Pr(u_{i,k} = 0) = 1 - f$. Thus, on average, we are using a different set of $N = fN_{full}$ cameras for each image frame.

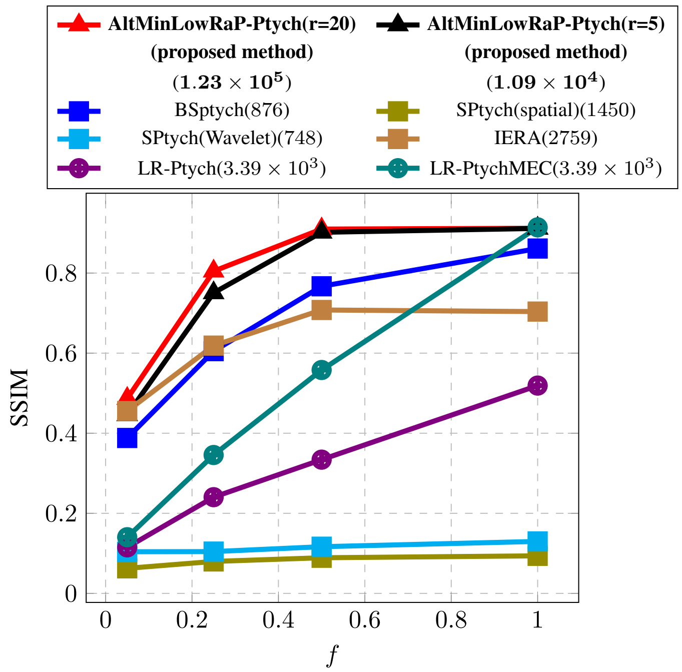

Fig. 2: *Comparison of **AltMinLowRaP-Ptych(Proposed Algorithm)** with existing ptychography algorithms on video "Bacteria". Running time shown in bracket (seconds)*

We use Structural Similarity Index (SSIM) [17] w.r.t. the ground truth image sequence as the metric for quality of reconstruction; higher SSIM means better recovery. All our plots display SSIM versus undersamping rate f for the various compared approaches. We used 4 values of f.

We set $T = 10$ and $T' = 10$ respectively for both AltMinLowRaP-Ptych and LR-Ptych. Also the number of iterations for Algorithm 2 is set to 50.

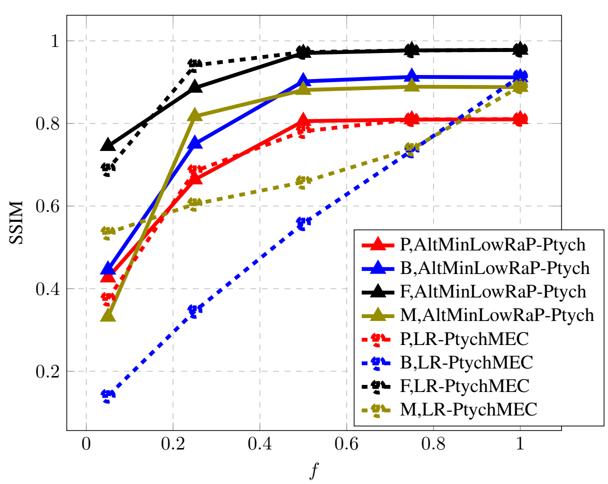

Fig. 3: *Comparison between accuracy of reconstructed frames by AltMinLowRaP-Ptych and LRPtych for all 4 videos "Plane"(P), "Bacteria"(B), "Fish"(F), "Mouse"(M).*

4.1. Proposed method versus other existing algorithms

As the first set of experiments we compare our proposed method with existing algorithms on the bacteria video. The result of this experiment can be seen in Fig. 2 for the bacteria ("B") video. Basic AltMinPhase for this problem [3] (referred to as "IERA" in the paper) uses 250 iterations. LR-Ptych and LR-PtychMEC [15, 4] consider LR structure as well while the other three algorithms make different types of sparsity assumptions [18]. Specifically, BSptych considers the whole video as a large matrix and assumes it is block sparse with sparsity level of 0.3. SPtych (spatial) and SPtych (Wavelet) consider the sparsity of each frame on spatial and wavelet domain correspondingly with sparsity level of 0.3. As it can be concluded from Fig. 2, sparsity for single frame does not provide recovery. IERA and BSptych have better results and BSptych shows slightly better performance than IERA due to assuming sparse structure. AltMinLowRaP-Ptych (the proposed method) shows significantly better performance compared to all existing algorithms in this experiment. Although the original version of AltMinLowRaP-Ptych needs longer running time, it is possible to reduce it to the same level of LR-Ptych by using $r = 5$, but more iterations of MEC (using $T' = 20$; and by gradually increasing the number of iterations for AltMinPhase T_b from 7 to 30 in different iteration of outer loop. With these changes, the error remains almost the same, but the time taken reduces drastically).

4.2. Comparison with LR-Ptych

Next we compare our proposed method with the second best approach from Fig. 2 which is LR-Ptych. Here the proposed algorithm uses $r = 5$, set T_b gradually increasing from 7 to 30 and $T' = 20$. Thus we can enable it to have roughly the same time complexity of LR-Ptych. As Fig 3 shows, AltMinLowRaP-Ptych outperforms LR-Ptych in terms of SSIM with the modeling error correction step. This is not as significant with video of "F" as result of LR-Ptych is also very good for this video. The superiority of our algorithm is also visible for the under-sampling case as well. This is specially the case for videos of "P","B", and "M" in comparison with performance of LR-Ptych. The reason behind this is better recovery of subspace coefficients in our approach.

5. CONCLUSIONS

We developed a modification of our recent AltMin based solution for Phaseless PCA (Low Rank Phase Retrieval) to provide a practical solution to undersampled dynamic Fourier ptychographic imaging. We compared the proposed algorithm with the state of the art phase retrieval (PR) and structured PR based solution approaches for this problem and showed that it outperforms or significantly outperforms most of them when compared on simulated measurements of real videos. As part of future work, we will develop a new and faster gradient-descent based solution to LRPR from our ongoing work [19] for solving this problem.

6. REFERENCES

[1] G. Zheng, R. Horstmeyer, and C. Yang, "Wide-field, high-resolution fourier ptychographic microscopy," *Nature photonics*, vol. 7, no. 9, pp. 739–745, 2013.

[2] S. Dong, R. Horstmeyer, R. Shiradkar, K. Guo, X. Ou, Z. Bian, H. Xin, and G. Zheng, "Aperture-scanning fourier ptychography for 3d refocusing and super-resolution macroscopic imaging," *Optics express*, vol. 22, no. 11, pp. 13586–13599, 2014.

[3] J. Holloway, M. S. Asif, M. K. Sharma, N. Matsuda, R. Horstmeyer, O. Cossairt, and A. Veeraraghavan, "Toward long-distance subdiffraction imaging using coherent camera arrays," *IEEE Transactions on Computational Imaging*, vol. 2, no. 3, pp. 251–265, 2016.

[4] G. Jagatap, Z. Chen, S. Nayer, C. Hegde, and N. Vaswani, "Sample efficient fourier ptychography for structured data," in *IEEE Transactions on Computational Imaging*, 2019.

[5] N. Vaswani, S. Nayer, and Y. C. Eldar, "Low rank phase retrieval," *IEEE Transactions on Signal Processing*, August 2017.

[6] S. Nayer, P. Narayanamurthy, and N. Vaswani, "Provable low rank phase retrieval," *IEEE Transactions on Information Theory*, vol. 66, no. 9, pp. 5875–5903, 2020.

[7] S. Nayer and N. Vaswani, "Sample-efficient low rank phase retrieval," *IEEE Transactions on Information Theory*, vol. 67, no. 12, pp. 8190–8206, 2021.

[8] T. Cacace, V. Bianco, and P. Ferraro, "Quantitative phase imaging trends in biomedical applications," *Optics and Lasers in Engineering*, vol. 135, pp. 106188, 2020.

[9] S. Lu, Y. Tian, Q. Zhang, X. Lu, and J. Tian, "Dynamic quantitative phase imaging based on ynet-convlstm neural network," *Optics and Lasers in Engineering*, vol. 150, pp. 106833, 2022.

[10] T. Bendory, R. Beinert, and Y.C. Eldar, "Fourier phase retrieval: Uniqueness and algorithms," in *Compressed Sensing and its Applications*, pp. 55–91. Springer, 2017.

[11] D. A. Barmherzig, J. Sun, P. Li, T. J. Lane, and E. Candes, "Holographic phase retrieval and reference design," *Inverse Problems*, vol. 35, no. 9, pp. 094001, 2019.

[12] F. Arab and M. S. Asif, "Solving fourier phase retrieval with a reference image as a sequence of linear inverse problems," in *2021 IEEE International Conference on Image Processing (ICIP)*. IEEE, 2021, pp. 2853–2857.

[13] E. J. Candes and B. Recht, "Exact matrix completion via convex optimization," *Found. of Comput. Math*, , no. 9, pp. 717–772, 2008.

[14] P. Netrapalli, P. Jain, and S. Sanghavi, "Low-rank matrix completion using alternating minimization," 2013.

[15] Z. Chen, G. Jagatap, S. Nayer, C. Hegde, and N. Vaswani, "Low rank fourier ptychography," *Proc. IEEE Int. Conf. Acoust., Speech, and Sig. Proc. (ICASSP)*, 2018.

[16] P. Netrapalli, P. Jain, and S. Sanghavi, "Phase retrieval using alternating minimization," in *Advances in Neural Information Processing Systems*, 2013, pp. 2796–2804.

[17] Z. Wang, A. C. Bovik, H. R. Sheikh, and E. P. Simoncelli, "Image quality assessment: from error visibility to structural similarity," *IEEE transactions on image processing*, vol. 13, no. 4, pp. 600–612, 2004.

[18] G. Jagatap and C. Hegde, "Fast, sample-efficient algorithms for structured phase retrieval," *Adv. Neural Inf. Proc. Sys. (NIPS)*, pp. 4924–4934, 2017.

[19] S. Nayer and N. Vaswani, "Fast and sample-efficient federated low rank matrix recovery from column-wise linear and quadratic projections," *arXiv preprint arXiv:2102.10217*, 2021.